IOSR Journal of Applied Physics (IOSR-JAP)
e-ISSN: 2278-4861.Volume 8, Issue 6 Ver. IV (Nov. - Dec. 2016), PP 38-49
www.iosrjournals.org

Structure, Electrical Conductivity and Dielectric Analysis of ZNO-Ag Phosphate Glasses

A.Langar[a], N.Sdiri[a*], H. Elhouichet[a,b], M.Ferid[a]

[a] *Laboratoire de Physico-Chimie des Matériaux Minéraux et leurs Applications, Centre National de Recherches en Sciences des Matériaux, B.P. 95 Hammam-Lif, 2050, Tunisia.*

[b] *Département de Physique, Faculté des Sciences de Tunis, Université de Tunis-ElManar ElManar 2092, Tunisia. Physics properties*

Abstract: *Silver zinc phosphate glasses with a composition (40-x/2) P_2O_5 – (40-x/2) Na_2O–20ZnO–x $AgNO_3$ (x = 5, 10 and 15 mol %) were prepared of the glasses via conventional melt-quenching technique. From the Raman spectrum, the structure of the glasses was analyzed. Conduction and relaxation mechanisms in these glasses were studied using impedance spectroscopy in a frequency range from 10 Hz to 13 MHz and a temperature range from 323 K to 623 K. The dependence of electrical data on frequency was analyzed in the framework of the Nyquist's plot and Jonscher's power law. The parameters of Nyquist's curves were calculated. The semicircles observed in the plots indicate a double relaxation process. This behavior can be modeled by an equivalent parallel RC circuit. The studied materials exhibit a significant contribution of grain and grain boundary effect to electrical conduction and to non-Debye relaxation process. The dc conductivity (σ_{dc}) follows Arrhenius behavior with temperature. The AC and dc conductivities of the samples were found to increase with the increase in temperature. The conductivity variation for P_2O_5-Na_2O-ZnO glasses doped with various concentrations of $AgNO_3$ was explained by the presence of ionic contribution. This suggests that the enhancement of conductivity is related to the thermally stimulated mobility of Ag^+ ions.*

The dielectric characterizations include measurements involving the variation of the dielectric constant as well as the dielectric loss with frequency. The dielectric studies show low values for the dielectric constant and loss at high frequencies. Dependence of the electrical modulus of the glasses on frequency and temperature presented a relaxation phenomenon.

Keywords: *Glasses; Impedance spectroscopy; Conduction; Dielectric.*

I. Introduction

The ionic conductivity of glasses has recently been investigated. This is thanks to their potential applications in solid state ionic devices **[1].** Among the different oxide glasses, ion conducting phosphate glasses are generally interesting owing to their numerous properties, such as high thermal expansion coefficient, low glass transition and softening temperatures **[2-4].**

Phosphate glasses have several technological applications. They can be used for making solid state electrolytes in solid state batteries, amorphous semi conductors, laser glasses and optoelectronic devices **[5].**

Furthermore, a special attention has been devoted to silver conducting glasses as candidates for solid electrolytes in silver cells. In order to improve the ionic conductivity of phosphate glasses, their structure was modified using a metal oxide, $AgNO_3$. The conductivity of these glasses depends on the movement of Ag^+ ions through the structure, so it is strongly affected by the structure. Indeed, the number of mobile ions is simply increased with the amount of $AgNO_3$ added into the glass former network, however the number of mobile ions is not dependent on the added $AgNO_3$ **[6].**

Impedance spectroscopy is one of the most powerful tools for the electrical characterization of solid materials. In fact, complex impedance, ac conductivity and dielectric relaxation can be measured by impedance spectroscopy. By studying the dielectric parameters of glasses such as dielectric constant, dielectric loss and ac conductivity over a wide range of frequencies, we get information about the insulating character, conduction behavior and the structural aspects of these materials. The charge transport properties in ion conducting glasses too are a current topic of research because of their potential applications in electrochemical cells and their technological applications in vacuum ultraviolet optics **[7].**

We have chosen silver ions because they are known for their high-conductivity, resistance against humidity and the possibility of being used in a large number of fields, such as biomaterials **[8].**

Although, a considerable number of studies on certain silver phosphate glasses are available still there is a lot of scope to investigate the role of silver ions especially in the presence of alkali metal and ZnO semiconductor. The role played by ZnO in dc electrical conductivity, in the entire composition range, is of great interest. The compositional dependence of ionic dc electrical conductivity and activation energy were compared with that of other traditional glasses.

In the present work, the effect of mixed glass formers on the ionic transport and dielectric properties of oxide glasses, with compositions (40-x/2) P_2O_5 – (40-x/2) Na_2O–20ZnO–x $AgNO_3$, are carried out in the frequency range 10 Hz - 13 MHz and at temperatures ranging from 323 K to 623 K. The ionic conduction and dielectric results in the pellets are also discussed.

II. Experimental procedure

Glasses of (40-x/2) P_2O_5 – (40-x/2) Na_2O–20ZnO–x $AgNO_3$ (x = 5, 10 and 15 mol %) were prepared by conventional melt quenching technique. Our samples are denoted NZAg5, NZAg10 and NZAg15 corresponding to $AgNO_3$ concentrations of 5, 10 and 15 mol%, respectively. P_2O_5, Na_2O, ZnO and $AgNO_3$ were taken as raw materials. All the starting chemical constituents have more than 99.9% purity. Required amounts of chemicals were thoroughly mixed in an agate mortar and melted in an electric furnace at 900°C for1h in a platinum crucible so that a homogeneously-mixed melt was obtained.

Immediately after the quenching, the glasses were annealed at 200°C (for 1h) and then slowly cooled until ambient temperature. The annealing process was made for the objective of minimizing the internal mechanical stress and obtaining glasses with good mechanical stability. The obtained glasses were cut and polished carefully in order to meet the requirements of measurements.

The glassy nature of the samples was confirmed by XRD studies using a D5000 Siemens Diffractometer with Cu-K_α line of a wavelength λ=1.5406 Å at a scanning rate of 1°/min, and 2θ was varied from a low angle to 70°.

The Raman spectrum was recorded using a Jobin Yvon spectrometer (Labram HR model) equipped with an Ar^+ laser. Impedance spectroscopy measurements were carried out at room temperature using an Impedance/Gain Phase Analyzer Solar-tron 1260 in the frequency range of 10Hz to 13MHz. For these measurements, gold electrodes were evaporated onto opposite sides of the glasses. The sample has the form of a disk with a diameter (d=9 mm) and a thickness (e=2 mm), on which gold electrodes were deposited by thermal evaporation in vacuum. The DC conductivity (σ_{dc}) measurements were carried out using a Keithely electrometer (Model 617) in the temperature range of 323–623 K. Silver paste electrodes were deposited on both faces of the polished samples.

III. Results and discussion

1. X-ray diffraction studies

The X-ray diffraction spectrum of the glass sample prepared with x = 10 mol% is shown in Fig.1. This sample was found to have a glassy form with a broad hump which is characteristic of amorphous nature.

2. Raman spectrum

Fig.2. presents the Raman spectrum of phosphate glasses. The spectrum is recorded in the frequency range 200 to 1200 cm^{-1}. In the present paper, the structure of phosphate glasses was analyzed from the hypothesis that the glass consists of P–O bonds existing in amorphous P_2O_5. Thus, the morphology of phosphate glasses revealed that the basic structural element of phosphate glasses is the (PO_4) tetrahedron. The structural units constituting phosphate network are presented by Q^n notation where n (n=1, 2, 3) is the number of bridging oxygen atoms in PO_4 group **[9]**.

As can be seen in Fig.2.the Raman Spectrum of phosphate glasses shows the most prominent bands at 736 cm^{-1}, 1040 cm^{-1} and 1360 cm^{-1} as well as less intense bands at 346 cm^{-1}, 490 cm^{-1}, 906 cm^{-1} and 1110 cm^{-1}. All these vibrations come from the groups of phosphate network and can sometimes be associated with the presence of zinc intermediate oxide.

The band at 346 cm^{-1} is assigned to torsional modes of phosphate polyhedral noted (δ_m (P-O-Zn)), in the presence of zinc as modifier. The band around 490 cm^{-1} is attributed to similar torsional modes noted (δ_f (P-O-Zn)), in the presence of zinc as a network former **[10]**.

The band at 736 cm^{-1} is associated to the symmetric vibration of bridging oxygen P-O-P, noted (υ_s (P-O-P), in Q^2 units and is in the long-chain metaphosphates. The vibration at 1040 cm^{-1} and 1110 cm^{-1} are correlated to the symmetric and asymmetric stretching mode of non-bridging oxygens (PO_2), noted respectively (υ_s (PO_2), Q^2) and (υ_{as} (PO_2), Q^2) **[11-13]**.

The band observed at 906 cm^{-1} is attributed to the symmetric vibrations in P-O links of orthophosphate groups (PO_4), noted (υ_s (PO_4), Q^0) **[14]**.

The band at 1360 cm^{-1} is related to the stretching mode of (P=O) in Q^3 units **[15]**.

3. Impedance analysis

Fig.3. shows the complex impedance plot for NZAg5, NZAg10 and NZAg15 glasses at a temperature T=260°C. The impedance data in this figure is fitted into two semicircles indicating the presence of two relaxation processes. A theoretical curve fitting and experimental data are measured. A good agreement between

the experimental and theoretical curves was attained. Fig.3. exhibits non-Debye behavior that depresses the center of the arc to be below the x-axis and the values for the imaginary and real parts are not symmetric.
This non-Debye type originates from ionic conduction among the random free energy barriers of localized atoms **[16]**.

This Figure is composed of two semicircles; a large one and a small one. The large one at high frequencies indicates the effect of the grain and the small one at low frequencies reflects the interfacial effect.
In addition, Fig.3 shows that the maximum of the Imaginary impedance spectra Z″ shifts towards higher frequencies with the increase in $AgNO_3$ content. The broad nature of the peaks can be interpreted as being the consequence of relaxation time distributions.

In order to analyze the impedance spectrum, it is useful to have an equivalent circuit model that provides an realistic representation of the electrical properties of the respective regions.
Each phase (grain or interfacial) acts as an independent layer of material, so the equivalent circuit model is simply two parallel RC circuits connected in series, as shown in the figure insets **[17]**.

If the impedances of grain and grain boundary solid electrolyte are semicircles with an equivalent circuit consisting of two parallel RC circuits connected in series, the semicircles in complex impedance Z″ vs. Z′ plots are depressed with their center below the real axis. Therefore, a constant phase element (CPE) may be used to replace the capacitor with a constant phase element (CPE) **[16]**.
The grain and grain boundary resistance are respectively given by the diameters of the high frequency and low frequency arcs.
The equivalent circuit can be expressed by the function:

$$Z^* = Z' + jZ'' = \left[\frac{1}{R} + \frac{1}{Z^*_{CPE}}\right]^{-1} \qquad (1)$$

Where the impedance of the CPE is given by **[18]**:

$$Z^*_{CPE} = \frac{1}{A_0(j\omega)^n} \qquad (2)$$

Where j is the imaginary unit (j^2= -1) and ω is the angular frequency (ω=2πf, f being the frequency), A_0 is a constant independent of frequency and in $F.cm^{-2}.s^{n-1}$ **[19]**, and n is an exponential index which is a measure of semicircle-depression (ranging between zero and unity). When the constant n = 1, CPE represents an ideal capacitor with a value $C = A_0$.
These semicircles were fitted by the software ORIGIN6.0 (Microcal Software, Inc. Northampton, Ma USA) based on the following relationships:

$$Z' = \frac{R_g(1+R_gA_{0g}\,\omega^{n_g}\cos(\frac{n_g\pi}{2})}{1+2R_gA_{0g}\,\omega^{n_g}\cos(\frac{n_g\pi}{2})+(R_gA_{0g}\omega^{n_g})^2} + \frac{R_{int}(1+R_{int}A_{int}\omega^{n_{int}}\cos(\frac{n_{int}\pi}{2})}{1+2R_{int}A_{int}\,\omega^{n_{int}}\cos(\frac{n_{int}\pi}{2})+(R_{int}A_{int}\omega^{n_{int}})^2} \qquad (3)$$

$$Z'' = -\left(\frac{(R_g)^2A_{0g}\,\omega^{n_g}\sin(\frac{n_g\pi}{2})}{1+2R_gA_{0g}\,\omega^{n_g}\cos(\frac{n_g\pi}{2})+(R_gA_{0g}\,\omega^{n_g})^2} + \frac{(R_{int})^2A_{int}\,\omega^{n_{int}}\sin(\frac{n_{int}\pi}{2})}{1+2R_{int}A_{int}\omega^{n_{int}}\cos(\frac{n_{int}\pi}{2})+(R_{int}A_{int}\omega^{n_{int}})^2}\right) \qquad (4)$$

Mathematical formalism is used to extract the parameters from the modeled equivalent circuit with the basis of complex impedance formula Z*.
Table 1 illustrates the best fitting values of equivalent circuit elements in the different samples. We observed that the values of grain and interfacial resistance decrease with the amount of silver. Moreover, the values of CPE_g exponent n_g and CPE_{int} exponent n_{int} decrease with the addition of $AgNO_3$.
On the other hand, Table 1 shows that with silver content, the values of n_g increase with the content of silver and approach 1. Therefore CPE_g tends towards an ideal capacitor.
The same equivalent values of circuit and resistance were observed by K. Srinivas et al **[20]**.

IV. AC Conductivity study

The measured values of impedance were used to study the behavior of AC conductivity of the prepared phosphate glasses are calculated by using the following relation **[21]**:

$$\sigma(\omega) = \frac{e}{S}\left(\frac{Z'}{Z'^2 + Z''^2}\right) \quad (5)$$

Where e is the sample thickness, and S is the electrode area used to measure the properties of the sample.
Fig.4 presents the dependence of AC conductivity on frequency for the NZAg10 glass at several temperatures. The dispersion in conductivity is well described by Jonscher power law of the form **[22]**.

$$\sigma_{AC}(\omega) = \sigma_{dc} + A\,\omega^{p} \quad (6)$$

Where σ_{dc} is the frequency dependent dc conductivity of the sample, A is a weakly temperature dependent quantity and p is the power law exponent which lies in the range ($0 < p < 1$).
A and p are parameters to be adjusted. Solid continuous lines indicate the fitting of conductivity data to the above equation.

It is observed from Fig.4 that conductivity remains almost constant in the low frequency range, whereas it exhibits dispersion at higher frequencies. The flat plateau region may be attributed to the long-range transport of mobile silver ions in response to the applied electric field, where only successful diffusion corresponds to the dc conductivity value, σ_{dc}. The dispersion behavior in conductivity is assigned to the microscopic nature of inhomogeneities with the distribution of relaxation phenomena through the distribution of energy barriers in the glasses **[23, 24]**.

This behavior of AC conductivity was observed by Andrea Mandanici et al. **[25]**. Further, as typical of ion conducting systems, conductivity is proportional to energy dissipation in the material, which can increase by several orders of magnitude at increasing frequency from hertz to the microwave frequency region **[26]**.
The electrical conductivity of phosphate glasses depends on the concentration of silver ions which are mobile charge carriers **[27]**.
Thus, the increase in conductivity with the increase in temperature is mainly due to the increase in the mobility of the Ag^+ ions. This can be easily explained with the help of Cluster Bypass model **[28]**.

$AgNO_3$ are well known modifier oxides and enter the glass network either by rupturing or by breaking up the P–O–P structures. In turn, the break-up of the P–O–P structures introduces coordinated defects, known as dangling bonds, along with non-bridging oxygen ions. It is also quite likely that Ag^+ ions cause a change from the pure covalent bonds of PO_4 cluster to the substantial admixture of the ionic component similar to Li–F **[29]**.
The values of σ_{dc}, A, and p obtained for the various glasses at room temperature are listed in Table 2 which shows that dc conductivity σ_{dc} increases with the increase in temperature. The slope (p) increases up to a value nearly equal to one, suggesting that a single power law could not describe the dependence of conductivity on frequency in the entire frequency range investigated **[30]**.
Such a behavior is often attributed to the inter-silver ion interactions influencing ac transport **[31]**.
On the other hand, for ionic conductivity, the power law exponent (p) may lie between 0.5 and 1, representing ideal long-range pathways and diffusion-limited hopping, which is the case in our work **[32]**.
The dependence of AC electrical conductivity (σ_{AC}) of the NZAg5, NZAg10, NZAg15 glasses on temperature at different frequencies is shown in Fig. 5. The electrical conductivity (σ_{AC}) of the material is thermally activated and obeys Arrhenius equation:

$$\sigma_{AC} = \sigma_0 e^{-\frac{E_{aAC}}{k_B T}} \quad (7)$$

Where E_a is the activation energy, k_B is Boltzmann's constant, σ_0 is the pre-exponential factor and T is the absolute temperature factor. Indeed, it is observed that AC conductivity of the material increases with the rise in temperature.

The activation energy for all samples is found to decrease with increasing frequency which is given in Table 3. Besides, it is found that the values of E_{aAC} decrease when the Ag amounts decrease. This can be possibly due to the increase of the applied field frequency and the enhancement of the electronic jumps between the localized states in the gap of ZnO site **[33]**.
In addition, the increase in AC conductivity with the increase in frequency can be attributed to the decrease in the ionic contribution for higher frequencies.
Nevertheless, the values of AC conductivity are low; the result can be due to the dispersions of nano conducting particles in a matrix. In fact, these values allow good penetration of electromagnetic waves in our prepared samples. Indeed, the penetration depth, δ, of electromagnetic radiation into a material is expressed by the equation **[34]**:

$$\delta = \sqrt{\frac{2}{\omega \mu_0 \sigma_{AC}}} \qquad (8)$$

Where ω is the angular frequency, 2πf, and μ_0 is the permeability of free space.

V. DC Conductivity study

The dependence of dc conductivity on temperature for NZAg5, NZAg10 and NZAg15 glasses is measured and plotted in Fig. 6 as Ln (σ_{dc}T) versus the reciprocal temperature according to Arrhenius equation:

$$\sigma_{dc} T = \sigma_0 e^{-\frac{E_{adc}}{k_B T}} \qquad (9)$$

Where σ_{dc} is dc conductivity, σ_0 is the pre-exponential factor, E_{adc} is the activation energy for dc conduction, k_B is the Boltzmann's constant and T is the absolute temperature of glasses.

The activation energy E_a is calculated from the slope of the linear plot. On the other hand, E_a is the activation energy for conduction whose value is some kind of average heights of the energy barriers that the ions must overcome in their jumps**[35]**.

Table 4 presents the activation energy for our glasses in comparison with other glasses.

From Fig. 6, it is observed that the dc conductivity of the prepared glasses was found to increase linearly with increasing both temperature and silver amount.

From Table 4, we note a slight difference in the activation energy with increasing silver amount. The increase in ionic conductivity of all the samples is almost entirely due to the fact that the activation energy for conduction E_{adc} decreases. Thus, the expansion of glass skeleton with the introduction of dopant ions into voids in the structure forming narrow pathways leads to lowering the activation energy. This, in turn, facilitates the easy migration of mobile Ag^+ ions **[38]**.

The result reveals the important contribution of Ag^+ ions to the ionic conductivity. Moreover, the feature may be explained by the large compressive stress caused by cation–cation and cation–anion interactions. In addition, the presence of PO_4 and highly modified glass structure accounts for the lowest activation energy.

Compared with other works, the activation energy of silver zinc phosphate glasses is in the same order as that of $30Na_2O–10MoO_3–60P_2O_5$ **[36]** and more than that of $27Na_2O–3Al_2O_3–70B_2O_3$ **[37]**.

The variation of dc conductivity contributions due to grains (σ_g) and interfacial (σ_{int}), with temperature is plotted in Fig. 7.

All the plots show two distinct activation energies. For all the samples, the contribution of grain boundary to conductivity is higher than that of grains. For the studied system, the increasing value of σ_{int} is ascribed to the increased interfacial trapping phenomena **[39]**.

The activation energies for conduction due to grains and grain boundaries were calculated and are given in Table 5. The activation energy is found to be less for grain conduction compared to interfacial conduction.

The activation energy for grain and interfacial is found to decrease with Ag amount. The feature can be explained by the semiconductor effect of ZnO which is more manifested in the presence of a potentially important ion Ag^+. The activation energy is found to be less for interfacial conduction compared to that of grain conduction.

VI. Dielectric analysis

We determined both the real part (resistive) and the imaginary part (reactive) of complex impedance spectroscopic parameters. In various frequency ranges, we calculated the complex permittivity □*□ □ □ □ □ given by **[40]**:

$$\varepsilon^*(\omega) = \varepsilon'(\omega) - j\varepsilon''(\omega) = \frac{1}{jC_0\left(Z' + jZ''\right)} \qquad (10)$$

Where ε'(ω) and ε''(ω) are the real part known as dielectric constant and imaginary part known as dielectric loss of the complex permittivity respectively. $C_0 = \varepsilon_0 A/e$ is the capacitance of the empty cell (ε_0=8.854 10^{-12}F m^{-1}, A is the cross-sectional area of the flat surface of the pellet and e is its thickness). Z' is the real part of impedance and Z'' is the imaginary part of impedance.

The dielectric constant values measured from the impedance data are plotted as a function of frequency at different temperatures for NZAg10 glass is shown in Fig. 8. At lower frequencies there is more variation of dielectric constant values, but at higher frequencies dielectric constant values remain constant. Thus, we observe a significant increase in the dielectric constant value at a lower frequency region with temperature. This can be explained on the basis of polarization mechanism existing in the sample. The constant decrease at higher frequencies is attributed to the existence of space charge polarization. Furthemore, the increased dielectric

constant value at lower frequencies region is related to the contribution from space charge/interfacial polarization. In addition, the increase in ε'(ω) with temperature is due to the weakening of binding force between molecules/atoms with the increase in temperature, permitting the molecules/atoms to vibrate more and more which in turn increase the polarization, hence increase in the dielectric constant ε'(ω) **[41].**
The dielectric constant values are found to be higher compared with other works' **[42].**
Fig. 9 shows the variation of dielectric constant with frequency for NZAg5, NZAg10 and NZAg15 glasses at T=260°C. In addition, it is observed that the value of ε'(ω) for NZAg10 glass is the largest. The decrease in ε'(ω) with the frequency of the prepared glasses is explained by the decreasing number of dipoles which contribute to polarization. At a higher frequency, the behavior of ε'(ω) presented in Fig. 9 leads the ionic and orientation polarizability to decrease. Moreover, the ionic polarizability results from the displacement of ions of opposite signs from their regular lattice sites. This arises from the applied electric field as well as from the deformation of the electronic shells. Indeed, the higher ε'(ω) values of these amorphous glasses at lower frequencies were explained by the presence of grain boundaries. Grain boundaries contain defects such as dangling bonds, vacancies, and vacancy clusters. Thus, the space charges can move under the application of an external field and when they are trapped by the defects, lots of dipole moments (space charge polarization) are formed **[43].**
The dielectric loss is given by **[44]**:

$$\tan(\delta) = \frac{Z'}{Z''} = \frac{\varepsilon''}{\varepsilon'} \qquad (11)$$

The dissipation factor as a function of frequency for different temperatures is shown in Fig. 10. The curves exhibit one broad absorption maxima in the frequency range $10^4 - 10^5$ Hz. The peak amplitude decreases and shifts towards higher frequencies with temperature, indicating the dielectric relaxation character of dielectric losses of the sample, which slows down at lower temperatures. The peak frequency gives an estimate of dielectric relaxation time (τ) which is expressed by **[45]**:

$$\tau = \frac{1}{\omega} = \frac{1}{2\pi f_{max}} \qquad (12)$$

The values of the relaxation time (τ) for NZAg10 at different temperatures are listed in Table 6. The (τ) value is found to be decreasing on increasing temperature, which is a typical semiconductor like behavior. Further, the relaxation process is temperature dependent **[46].**
Accordingly, low losses at high frequencies imply that the prepared glasses are potential candidates for microwave devices **[47].**

VII. Electric modulus analysis

The electrical modulus formalism was used for a better description of the dynamic processes in the present glass system. This formalism is appropriate to identify phenomena such as electrode polarization and bulk phenomenon such as average conductivity relaxation times **[48].**
The complex electric modulus was determined by the following relation **[49]**:

$$M^* = M'(\omega) + jM''(\omega) \qquad (13)$$

Where:
$M' = -\omega C_0 Z''$ is the real part of the electric modulus, $M'' = \omega C_0 Z'$ is the imaginary part of the electric modulus, ω is the angular frequency ($\omega = 2\pi f$) and C_0 is the geometrical capacitance.
Dependence of $M'(\omega)$ and $M''(\omega)$ on frequency at different temperatures for NZAg10 glass is presented in Fig.11 and Fig.12. At a low frequency, we have observed a very low value (approximately zero) of the real part of the electric modulus M' and a dispersion at high frequency. This phenomenon may be due to the short range mobility of charge carriers and the ease of migration of conducting ions **[50].**
As the frequency is increased, M' represents a dispersion tending to M_∞ at higher frequencies. It can be attributed to the fact that at a high frequency the electric field changes so rapidly that the ions can move only within their potential wells **[51].**
From Fig.12, the peak in the imaginary part of the modulus is found to have shifted towards a higher frequency with the increase of temperature and is related to the thermally activated ion dynamics of the glass. The presence of relaxation-peaks in the M" plot indicates that the samples are ionic conductors **[52].**
The spectra describe two regions. The frequency region below ω_{max} determines the range in which charge carriers are mobile over long distances and it is due to the hopping of ions. For the region above ω_{max}, the carriers are confined their to potential wells and are mobile over short distances associated with polarization process **[53].**

VIII. Conclusion

Phosphate glasses with different concentrations of $AgNO_3$ (ranging from 5 to 15 mol%) were prepared by quenching technique. The presence of a broad band in XRD pattern demonstrates the amorphous nature of the samples. The Nyquist's plots showed the presence of two relaxation processes with a non-Debye type nature is confirmed. So, they can be modeled to an equivalent circuit consisting of two parallel RC circuits connected in series.

The activation energy and the conductivity of the system were calculated. The electric AC conductivity obeys to the Jonsher's law. The activation energy E_a was found to decrease with silver content. The dc conductivity followed Arrhenius law and increased with increasing both temperature and silver amount. In addition, the increase in conductivity in the prepared glasses is mainly due to Ag^+ ions conduction. Thus, the increase in the mobility of Ag^+ ions results from the formation of new non-bridging oxygen atoms providing more opened-up channels for Ag^+ conductions at higher temperatures.

At higher frequencies, the dielectric constant is found to be constant and low. The decrease in the dielectric constant values with the frequency of the samples is explained by the decreasing number of dipoles which contribute to polarization.

Imaginary modulus spectra confirmed that the samples are ionic conductors.

Through their good electrical conductivity and interesting dielectric constants with low losses, silver zinc phosphate glasses can be used in sustainable energy storage systems, chemical sensors or advanced electrochromic devices.

References

[1]. L F Maia and A C M Rodrigues *Solid State Ionics* **168** 87-92 (2004).
[2]. R Pires, I Abrahams, T G Nunes and G E Hawkes *J. Non-Cryst. Solids* **337** 1-8 (2004).
[3]. J L Nowinski, M Ksiezopolski, J E Garbarczyk and M Wasiucionek *J. Power Sourc* **173** 811-815 (2007).
[4]. S S Sastry, B R Venkateswara Rao and T Vishwam *Indian J. Phys* **89** 73 (2015).
[5]. S S Das, B P Baranwal, C P Gupta and P Singh *J. Power Sourc* **114** 346-351(2003).
[6]. A Moguš-Milanković, L Pavić, S T Reis, D E Day and M Ivanda *J. Non-Cryst. Solids* **356** 715–719(2010).
[7]. Salih V, Franks K, James M, Abrahams I, Hastings GW and Knowles JC *J.Mater.Sci* **11** 615–620(2000).
[8]. R Ciceo-Lucacel and I Ardelean *J.Non-Cryst.Solids* **353** 2020–2024 (2007).
[9]. S Sreehari, M V V K S Prasad , B R Venkateswara Rao and J Sivaramakrishna *Indian J. Phys* **89** 1169-1175 (2015).
[10]. R K Brow et al *J. Non-Cryst. Solids* **191** 45-55(1995).
[11]. T Jermoumi, M Hafid, N Niegisch, M Mennig, A Sabir and N Toreis *Mater. Res. Bull* **37** 49-57(2002).
[12]. K Suzuya, K Itoh, A Kajinami and C K Loong *J. Non-Cryst. Solids* **345 et 346** 80-87(2004).
[13]. A Santic, A Mogus-Milankovic, K Furic, V Bermanec, C W Kim and D E Day *J. Non-Cryst. Solids* **353** 1070-1077 (2007).
[14]. R L Frost *Spectrochim. Acta A* **60** 1439-1445 (2004).
[15]. R K Brow *J. Non-Cryst. Solids* **263 et 264** 1-28 (2000).
[16]. J Liu, C G Duan, W G Yin, W N Mei, R Smith and J R Hardy *J. Chem. Phys* **119** 2812 (2003).
[17]. J Jiang, T J Zhang, B S Zhang and H Mao *J. Electroceram* **21** 258 (2008).
[18]. G Friesen, M E Ozsar and E Dunlop *Thin Solid Films* **361-362** 303-308 (2000).
[19]. Jean Baptiste Jorcin, Mark E Orazem, Nadine Pébère and Bernard Tribollet *Electrochimica Acta* **51** 1473–1479 (2006).
[20]. K Srinivas, P Sarah and S V Suryanarayana *Bull. Mater. Sci* **26** 247–253(2003).
[21]. M Pant, D K. Kanchan, P Sharma and M S Jayswal *Mater Sci & Engg B* **149** 18-25 (2008).
[22]. A K Jonscher *Nature* **267** 673-679 (1977).
[23]. Saroj Rani, Sujata Sanghi, Neetu Ahlawat and Ashish Agarwal *Journal of Molecular Structure* **1098** 1-11 (2015).
[24]. S Rani, S Sanghi, A Agarwal and N Ahlawat *J. Mater. Sci* **44** 5781-5787 (2009).
[25]. Andrea Mandanici, Anna Raimondo, Mauro Federico, Piercarlo Mustarelli, Cristina Armellini and Francesco Rocca *J. Non-Cryst. Solids* **401** 254-257 (2014).
[26]. M Cutroni, A Mandanici, P Mustarelli and C Tomasi *Solid State Ionics* **154-155** 713- 717 (2002).
[27]. F M Ezz Eldin, N A El Alaily *Mater Chem Phys* **52** 175-179 (1998).
[28]. M D Ingram, M A Mackenzie, W Muller and M Torge *Solid State Ionics* **28-30** 677-680 (1988).
[29]. K Sambasiva Rao, M S Reddy, VR Kumar and N Veeraiah *Mater. Chem. Phys* **111** 283-292 (2008).
[30]. K Funke et al *J. Phys. Chem* **4** 3155–3167 (2002).
[31]. S Muthupari, S Lakshmi Raghavan, and K J Rao *J. Phys. Chem* **100** 4243 (1996).
[32]. K A Mauritz *Macromolecules* **22** 4483–4488(1989).
[33]. A M Farid and A E Bekheet *Vacuum* **59** 932-939 (2000).
[34]. A G Ramm *Physics Letters A* **360** 735–741 (2007)**.**
[35]. A Costantini, A Buri and F Brand *Solid State Ionics* **67** 175-178 (1994).
[36]. M Nagarjuna, T Satyanarayana, Y Gandhi and N Veeraiah *J. Alloys Compd* **479** 549-556 (2009).
[37]. H Doweidar, Y M Moustafa, S Abd El-Maksoud and H Silim *Mater. Sci. Eng. A* **301** 207-212 (2001).
[38]. J Swenson and L Borjesson *Phys. Rev. Lett* **77** 3569 (1996).
[39]. M Cutroni, A Mandanici, P Mustarelli and C Tomasi *Solid State Ionics* **154– 155** 713– 717 (2002).
[40]. V Raja, A K. Sharma and V V R Narasimha Rao, *Mater. Lett* **58** 3242-3247 (2004).
[41]. Sanjaya Brahma, R N P Choudhary and A K Thakur *Physica B* **355** 188-201 (2005).
[42]. C Bouzidi, N Sdiri, A Boukhachem, H Elhouichet and M Ferid *Superlattices and Microstruct* **82** 559–573 (2015).
[43]. A A Bahgat and Y M Abou-Zeid *J. Phys. Chem. Glasses* **42** 361-370 (2001).
[44]. M H Bhat, M Kandavel, M Ganguli and K J Rao *Bull. Mater. Sci* **27** 189-191 (2004).
[45]. L Affleck and C Leach *J. Eur. Ceram. Soc* **25** 3017-3020 (2005).
[46]. M R Ranga raju and R N P Choudhary *Indian Journal of Eingineering & Materials Sciences* **15** 137-146 (2008).
[47]. Nobre MAL and Lanfredi S *Catal Today* **78** 529 (2003).
[48]. R A Gerhardt *J. Phys. Chem. Solids* **55** 1491-1506 (1994).

[49]. A Šantić, C W Kim, D E Day and A Moguš-Milanković *J. Non-Cryst. Solids* **356** 2699-2703 (2010).
[50]. Damian C Onwudiwe, Tanvir Arfin and Christien A Strydom *Superlattices and Microstruct* **81** 215-225 (2015).
[51]. S W Martin and A Angell *J. Non-Cryst. Solids* **83** 185-207 (1986).
[52]. A Ben Rhaiem, F Hlel, K.Guidara and M Gargouri *J Alloy Compd* **463** 440-445 (2008).
[53]. Alo Dutta, T P Sinha, P Jena and S Adak *J Non-cryst Solids* **354** 3952-3957 (2008).

Figures captions

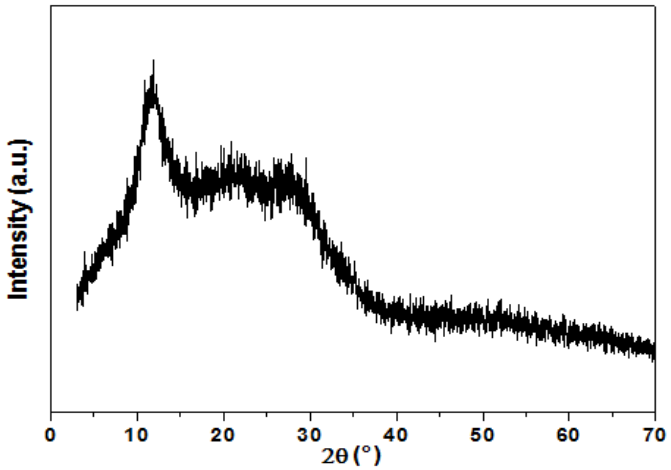

Fig. 1. X-ray diffraction pattern of the sample with x = 10 mol%.

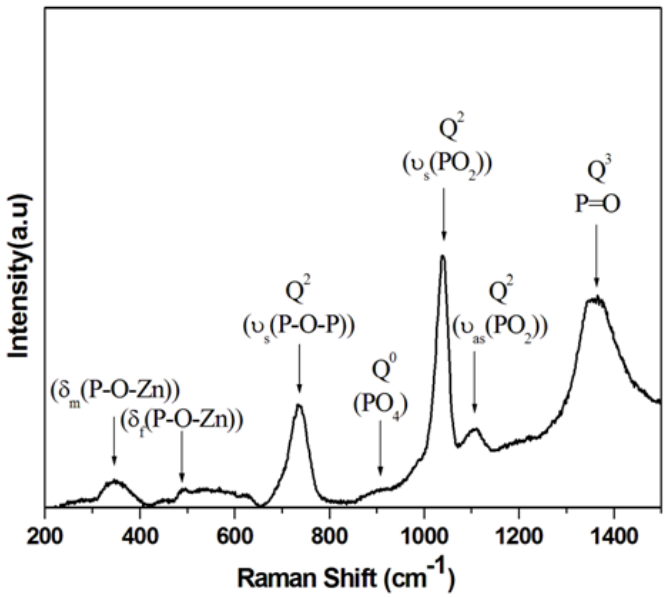

Fig. 2. Raman spectrum of phosphate glass.

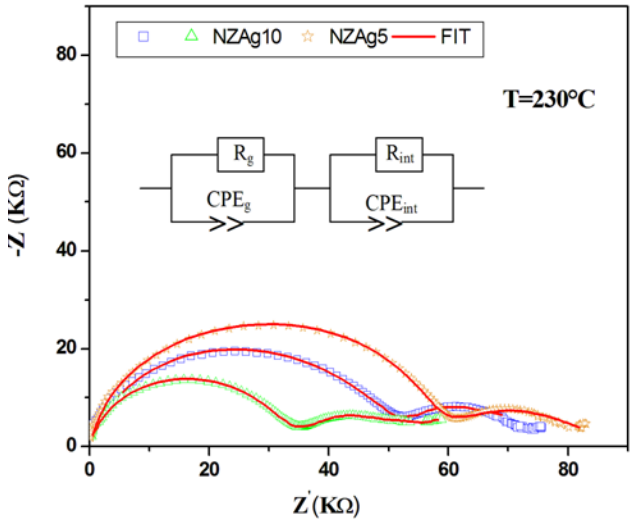

Fig. 3. Experimental and theoretical impedance diagrams of the NZAg5, NZAg10 and NZAg15 glasses with inset the corresponding equivalent circuit at temperature T=230°C.

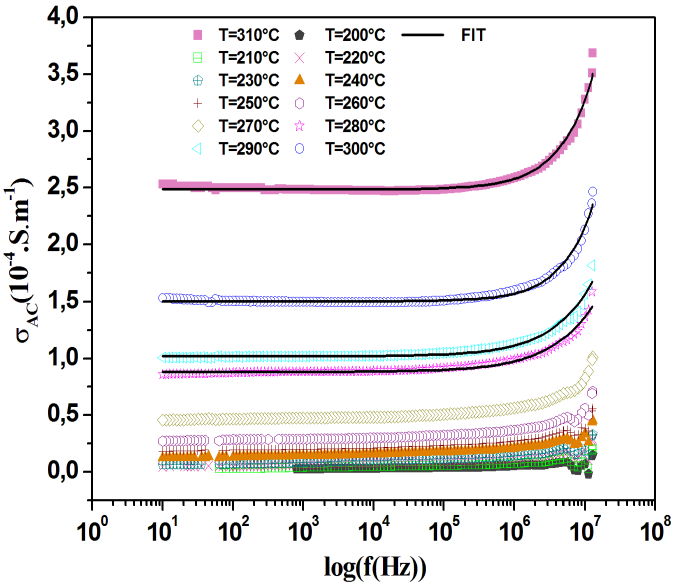

Fig. 4. Variation of the AC conductivity (σ_{AC}) of NZAg10 glass versus frequency (f) at different temperatures.

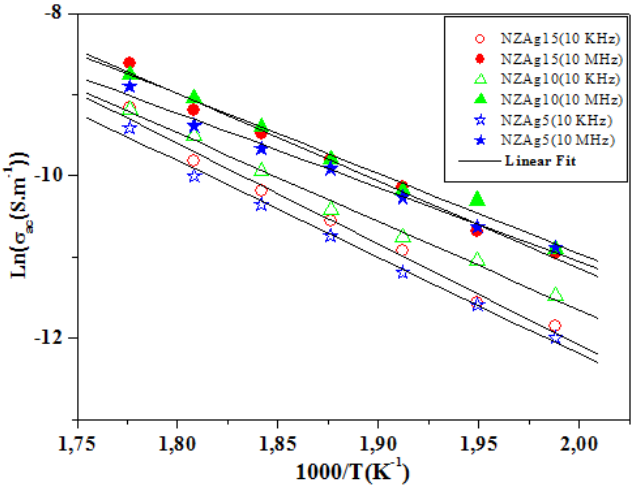

Fig.5. Temperature dependence of AC conductivity (σ_{AC}) of the NZAg5, NZAg10 and NZAg15 glasses at different frequencies.

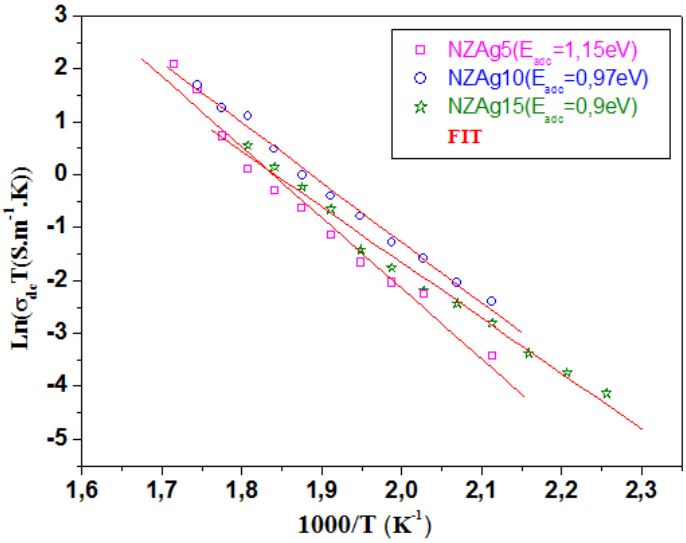

Fig. 6. Arrhenius relation of Ln (σ_{dc}T) versus 1000/T for NZAg5, NZAg10 and NZAg15 glasses.

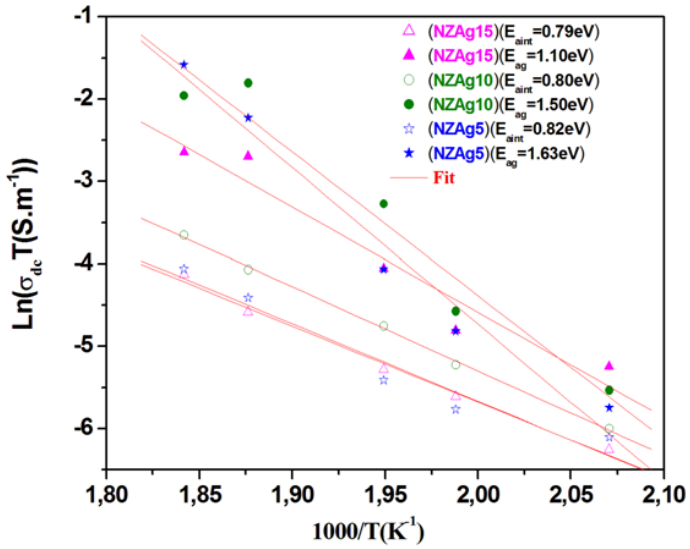

Fig.7. Arrhenius relation of Ln (σ_{dc}T) versus 1000/T for NZAg5, NZAg10 and NZAg15 glasses for grain (σ_g) and interfacial (σ_{int}).

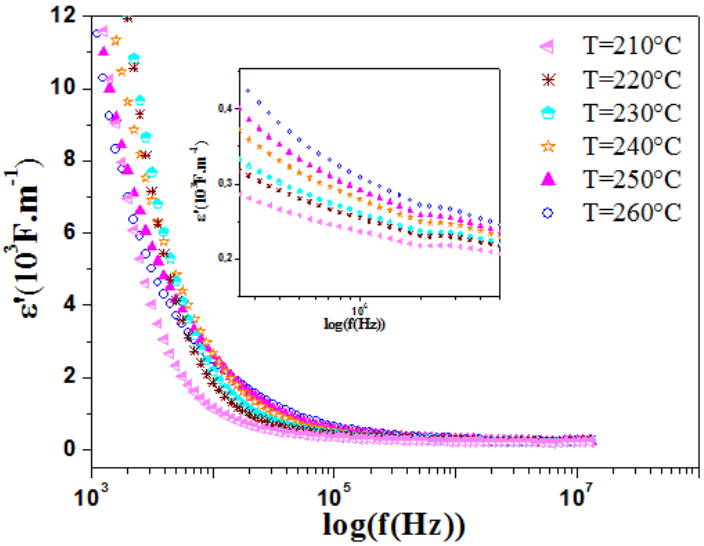

Fig.8. The frequency dependence curves of dielectric constant ε'(ω) of NZAg10 glass at different temperatures.

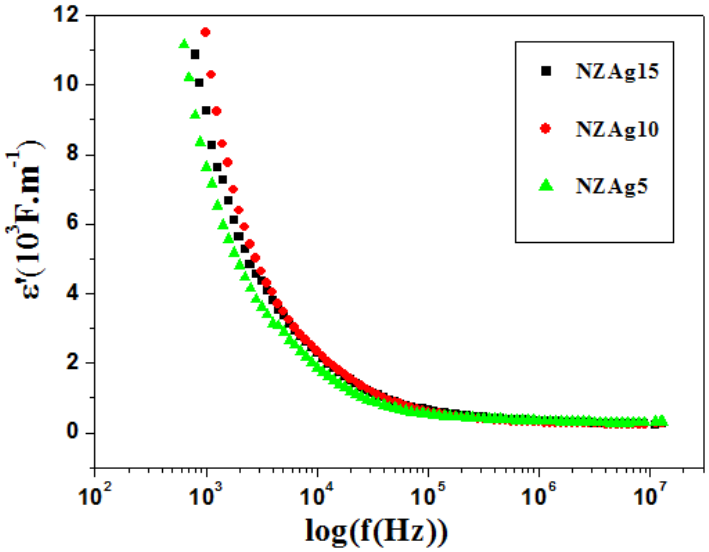

Fig.9. The frequency dependence curves of dielectric constant ε'(ω) at T=260°C for NZAg5, NZAg10 and NZAg15 glasses.

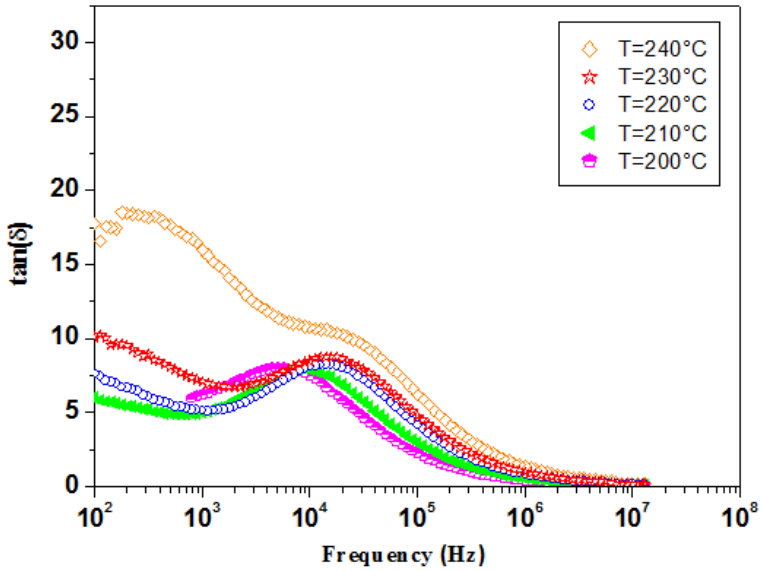

Fig.10. Variation of loss tan(δ) versus frequency for NZAg10 glass at different temperatures.

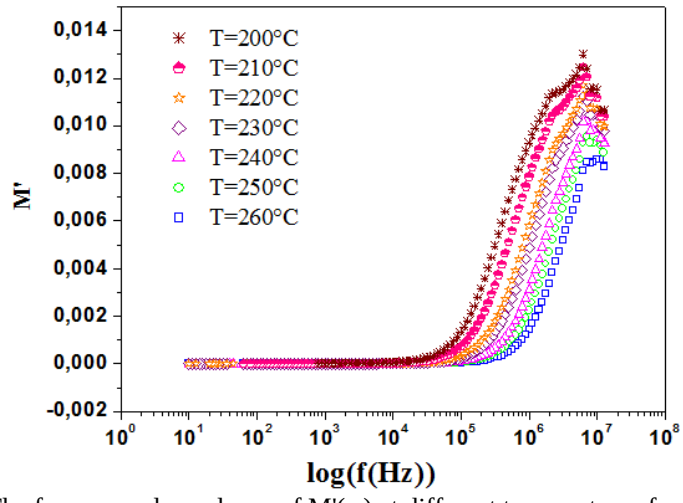

Fig.11. The frequency dependence of M'(ω) at different temperatures for NZAg10 glass.

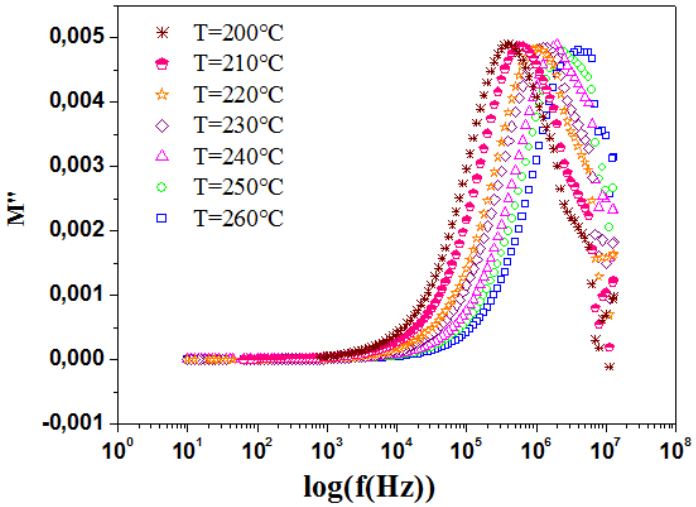

Fig.12. The frequency dependence of M"(ω) for NZAg10 glass at different temperatures.

Tables captions

Table 1: The best fitting values of equivalent circuit elements in Fig. 3 in different host materials.

Host materials	Rg(KΩ)	$A_{0g}(10^{-11}F.cm^2.s^{n-1})$	n_g	R_{int}(K□)	$A_{0int}(10^{-7}F.cm^2.s^{n-1})$	n_{int}
NZAg5	61.29	4.06	0.88	82.48	2.02	0.61
NZAg10	35.19	3.08	0.90	53.70	7.34	0.45
NZAg15	52.34	5.89	0.86	75.58	14.23	0.40

Table 2: Values of the dc conductivity (σ_{dc}), (A), and the slope (s), for NZAg10, determined at different temperatures.

Temperature (°C)	$\sigma_{dc}\left(10^{-4}(S.m^{-1})\right)$	A	s
280	0 .9	3.31×10^{-10}	0.73
290	1	2.88×10^{-10}	0.75
300	1.5	9.88×10^{-11}	0.82
310	2.5	2.19×10^{-11}	0.93

Table 3: Activation energy of AC conductivity at (10 KHz) and (10 MHz) for NZAg5, NZAg10 and NZAg15 glasses.

Samples	$E_{a(AC)\,(10\,KHz)}$ (eV)	$E_{a(AC)\,(10MHz)}$ (eV)
NZAg 5	1.02	0.76
NZAg10	0.95	0.85
NZAg15	1.07	0.96

Table 4: The activation energy and composition of the prepared glasses compared with other glasses.

Host materials	NZAg 5	NZAg 10	NZAg 15	$30Na_2O–10MoO_3–60P_2O_5$ [36]	$27Na_2O–3Al_2O_3–70B_2O_3$ [37]
Activation energy (eV)	1.15	0.97	0.90	0.84	0.77

Table 5: The activation energy of grain and grain boundary for NZAg5, NZAg10 and NZAg15 glasses.

Host materials	NZAg 5	NZAg 10	NZAg 15
Activation energy of interfacial (eV)	0.82	0.80	0.79
Activation energy of grain (eV)	1.63	1.50	1.10

Table 6: Values of the relaxation time (τ) for NZAg10 at different temperatures.

Temperature (°C)	200	210	220	230	240
τ (s)	2.05×10^{-4}	1.16×10^{-4}	6.33×10^{-5}	5.96×10^{-5}	4.59×10^{-5}